Beam loss detection based on generation of Cherenkov light in optical fibers in the CERN Linear Electron Accelerator for Research

S. Benítez,[*,†] B. Salvachúa, and M. Chen[†]
CERN, Geneva, Switzerland

(Received 3 November 2023; accepted 22 April 2024; published 28 May 2024)

Cherenkov optical beam loss monitors (oBLMs) based on optical fibers are a revolutionary achievement among the monitoring systems in particle accelerators. Due to the nature of the Cherenkov phenomenon and the intrinsic characteristics of optical fibers, the photon production and fiber light transmission need to be studied to deduce the total amount of Cherenkov photons detected by the photosensors attached at the end of the system. Simulations of the Cherenkov oBLM detector system have been implemented using the FLUKA software with postprocessing considering the light attenuation and capture factors in the optical fiber. In addition, the study includes the longitudinal beam loss localization of the controlled beam losses produced along the CERN Linear Electron Accelerator for Research (CLEAR) test facility line. In this paper, the Cherenkov photon detection by an oBLM installed in the CLEAR facility is simulated, analyzed, and compared with experimental data.

DOI: 10.1103/PhysRevAccelBeams.27.052901

I. INTRODUCTION

One of the most promising beam loss detection systems for accelerators is the Cherenkov optical beam loss monitor (oBLM). It is based on the use of optical fibers coupled to photosensors, one at each fiber end. This setup is capable of continually measuring beam losses over long distances in real time. The particle shower, resultant of a beam loss, arrives at the fiber and interacts with the silica, generating Cherenkov photons instantaneously, which travel along the fiber to be collected by the photosensors. This technology is under development in several institutions worldwide. For instance, the Linac Coherent Light Source (LCLS) in the Stanford Linear Accelerator (SLAC) [1] or the Free Electron Laser Hamburg (FLASH) in Deutsches Elektronen-Synchrotron (DESY) [2] has promoted Cherenkov BLMs in their beam loss detection systems. At CERN, previous studies were carried out at the CLIC Test Facility 3 (CTF3) [3].

For a comprehensive understanding of system behavior, simulations of particle showers and their interactions with accelerator components are essential. The FLUKA [4] software uses the Monte Carlo (MC) method to obtain numerical results by repeating random sampling, and FLAIR [5] can be used as its interface. It simulates particle interaction and transport in any material. Through FLUKA and FLAIR, simulations were able to accurately determine the charged particles fluence in the optical fiber installed in the CLEAR line. However, as yet, a model for estimating the number of Cherenkov photons generated inside optical fibers has not been reported. In this paper, we describe a complete model for Cherenkov light generation and propagation in optical fibers. Furthermore, we examine how light is captured and transported along the fiber as well as the impact of attenuation. Simulations and modeled results of beam loss detection and Cherenkov photon generation by an oBLM used in CLEAR are then compared and discussed with experimental data.

II. CHERENKOV LIGHT GENERATION

As mentioned previously, Cherenkov detectors are widely used in accelerators due to their fast detection properties. Specifically, quartz optical fibers are the most common devices for continuous detection and localization of beam losses over long distances. In addition, fibers are insensitive to extreme temperatures, x rays, or magnetic fields, can withstand high doses of radiation without being damaged, and are practically noninvasive systems. The Cherenkov phenomenon occurs when high-energy charged particles pass through a polarizable medium (quartz) at a greater speed than the phase velocity of the light in that medium. The number of generated photons N, for a given wavelength λ and per particle traveled path length x, is given by Eq. (1) [6,7]:

[*]sara.benitez.berrocal@cern.ch
[†]Also at University of Huddersfield, Huddersfield, United Kingdom.

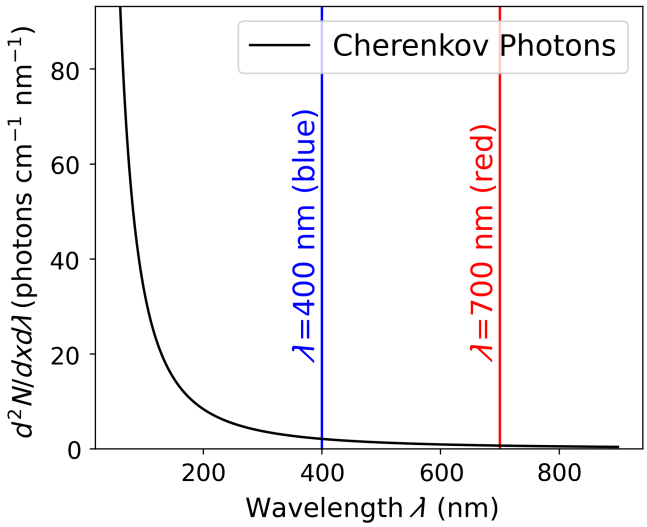

FIG. 1. Cherenkov emission spectrum [8].

$$\frac{d^2N}{dxd\lambda} = \frac{2\pi\alpha z^2 \sin^2\theta_c}{\lambda^2}, \tag{1}$$

where α is the fine structure constant, z is the particle charge, and θ_c is the photons' emission angle. For high-relativistic particles, the Cherenkov angle, θ_c, can be approximated as $\theta_{c,max} \approx \arccos(1/n)$. For silicon optical fibers with refractive index $n \approx 1.46$, the angle of maximum emission is $\theta_{c,max} \approx 47°$. Figure 1 shows the Cherenkov spectrum calculated from Eq. (1). It can be noticed that Cherenkov radiation dominates the ultraviolet (UV) range and decreases with wavelength, being almost nonexistent in the infrared (IR) range.

A. Modelling in optical fibers

The modeling of the oBLM includes the simulation of photons in the optical fiber as well as the capture, attenuation, and transport to the photosensors. The first part starts with the simulation of the number of photons generated in a Cherenkov oBLM installed along the CERN Linear Electron Accelerator for Research (CLEAR) [9] geometry. The interactions of particle showers into the optical fiber along the beam line were reproduced with the FLUKA transport code. Once the high-energetic charged particles reaching the fiber were tracked, a postprocessing of the data was performed to calculate the Cherenkov photons generated, implementing the attenuation and capture factors. The combination of these processes represents the modeling of Cherenkov light in fiber presented here [10,11].

Only a fraction of the initially generated photons will be detected because the intrinsic characteristics of the optical fibers reduce the collection efficiency. Two principal factors are driving this reduction: light capture and attenuation. After the polarization of the quartz molecules by the high-energetic charged particles, a portion of the Cherenkov photons generated will be captured and transported along the fiber thanks to the total reflection phenomenon. The so-called capture factor determines the total number of captured and propagated Cherenkov photons potentially reaching the photosensor at the end of the fiber. The capture factor F_{cap} has been calculated as [12]:

$$F_{cap} = \frac{1}{\pi}\arccos\left(\frac{\beta\sqrt{n_{co}^2 - NA^2} - \cos\phi}{\sin\phi\sqrt{\beta^2 n_{co}^2 - 1}}\right), \tag{2}$$

where $\beta = v/c$ is the velocity factor, being v the velocity of the high-energetic charged particle (for the following approximated to $\beta \to 1$), NA is the numerical aperture of the optical fiber, defined as $NA = \sqrt{n_{co}^2 - n_{cl}^2}$, with n_{co} and n_{cl} as the core and cladding refraction indices, respectively [13], and ϕ is the incident angle between the fiber axis and the charged particle track in the fiber [14]. The probability of the photons reaching the photosensors depending on the angles of capture presented in Fig. 2. For silica fibers, the maximum probability values are around the Cherenkov angles $\theta \approx \pm 47°$, as expected.

Intrinsic light absorption, impurities, and light scattering due to microscopic fluctuations in the material reduce the optical signal inside the fibers [11]. Optical fibers with length L have signal power $P(L,\lambda)$ defined as

$$P(L,\lambda) = P(0,\lambda) \times 10^{-\frac{\nu L}{10}}, \tag{3}$$

where ν is the attenuation coefficient expressed in. This coefficient can be described by the sum of the three main light attenuation contributions in an optical fiber: ultraviolet, infrared absorption bands, and Rayleigh scattering. Then

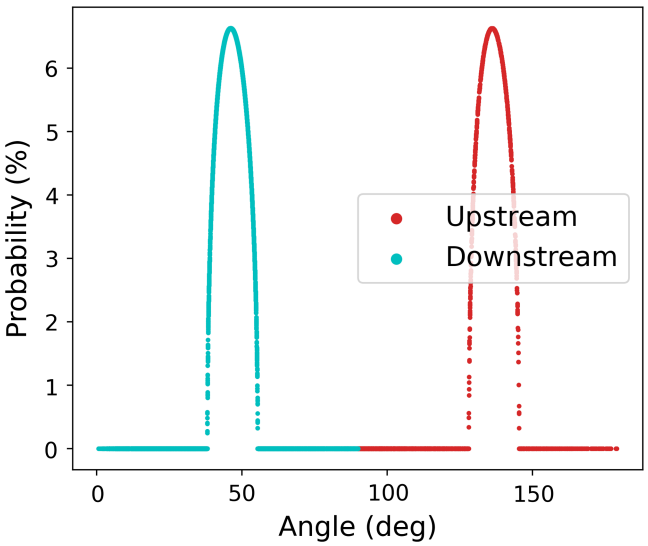

FIG. 2. Probability of photon capture with respect to the angles of incidence for the parameters: $\beta \approx 1$, NA = 0.22, and $n_{co} = 1.46$ [8].

$$\nu = \nu_{\mathrm{UV}} + \nu_{\mathrm{Rayleigh}} + \nu_{\mathrm{IR}}. \tag{4}$$

The used silicon photomultipliers (SiPMs), coupled to both ends of the fiber, work within the wavelength range [290, 900] nm with maximum detection at ≈450 nm, where the dominant regime is the Rayleigh scattering. The IR radiation absorption is effective around 1700 nm and UV absorption will primarily affect the measurements in the 150–250 nm spectral region [15]. The effect on the Rayleigh scattering can be described as [16]:

$$\nu = \nu_{\mathrm{Rayleigh}} \simeq \frac{A_{\mathrm{R}}}{\lambda^4} \tag{5}$$

being A_{R} the Rayleigh scattering coefficient, and for pure silica, $A_{\mathrm{R}} = 0.83$ [dB μm^4/km]. The attenuation factor $\epsilon_{\mathrm{att}} = P(L)/P(0)$ for different fiber lengths is shown in Fig. 3. Light attenuation is strongly dependent on the wavelength and the length of the fibers. It is possible to observe how the wavelength range between [200, 400] nm gets significantly subtracted in longer fibers.

For the photons at the fiber extremity N_{end}, an analytical solution can be obtained by combining Eq. (1), (2), and the attenuation factor ϵ_{att} to

$$N_{\mathrm{end}} \approx \int \frac{d^2N(x,\lambda)}{dxd\lambda}\epsilon_{\mathrm{att}}(\lambda, L)F_{\mathrm{cap}}(\phi)dxd\lambda. \tag{6}$$

As example, in an experimental scenario involving protons (where $z = 1$) passing through a silica fiber and generating photons at a Cherenkov angle of $\theta = 47°$, the integration of Eq. (1) over a wavelength range of [400–700] nm leads to an estimated photon yield of around 26 photons/mm/proton, meaning that we would get 26 photons per millimeter of a proton path length in the material.

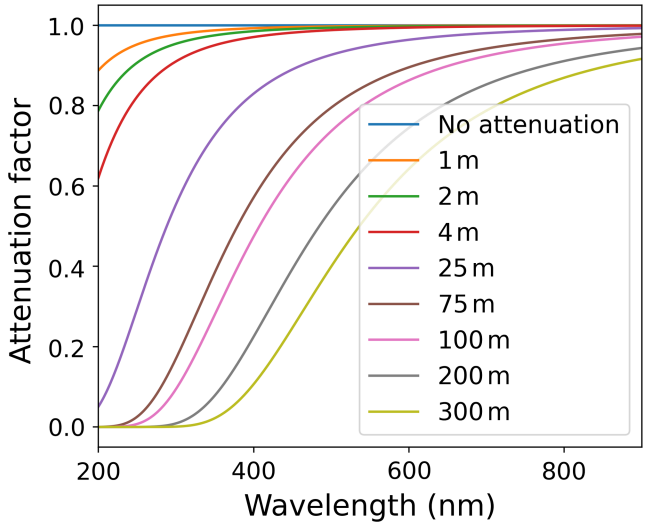

FIG. 3. Attenuation factor as a function of the wavelength for several fiber lengths [8].

However, when photons need to travel 100 m distance inside the fiber, following Eq. (6), the yield decreases to about 1 photon/mm/proton. Note that any type of high energetic charged particle may produce this phenomenon, and only for simplicity, we have specified a proton case. It should be noted that the photon detection efficiency (PDE) of the selected photon sensor is not considered in this calculation, as the focus is on the localization of losses. For a more accurate analysis of loss quantification, this could be considered by applying the PDE curves provided by the manufacturer to the simulations.

B. Localization of beam losses

With the presented setup of a fiber stretched along the accelerator beam line, readout by two photosensors at its extremities, the localization of beam losses is possible. This paper contrasts the results related to the beam loss localization from simulations and experimental data to validate the oBLM system.

The signal arrival timing varies depending on the location of beam losses within the fiber. By using a specific beam loss location as a reference point, it becomes possible to compute the time shifts for beam losses that happen at various positions. The equations for the differences in arrival times, denoted as Δt_{down} and Δt_{up}, at the downstream [Eq. (7a)] and upstream [Eq. (7b)] ends respectively, account for two beam losses occurring at different fiber locations, as outlined in [8]:

$$\Delta t_{\mathrm{down}} = \frac{\Delta x}{c}(1 - n) \quad \text{and} \tag{7a}$$

$$\Delta t_{\mathrm{up}} = \frac{\Delta x}{c}(1 + n), \tag{7b}$$

where Δx is the distance between the beam loss locations on the optical fiber, n is the average refractive index (for silica material $n = 1.46$), and $c = 0.3$ m/ns is the speed of light in vacuum. It is worth mentioning that Eqs. (7a) and (7b) exclusively focus on loss location measurement using only the timing information and not the signal amplitude. The goal of this installation is not the quantification of beam losses.

In order to quantify loss levels, at least three calibration factors would need to be assessed: (a) the capture factor, which depends on the angle of incidence of the secondary particles or losses on the fiber, (b) the attenuation factor depending on the distance from the loss location to the photosensors, which also depends on the wavelength, and (c) the radiation-induced attenuation factor that depends on the loss pattern along the fiber. In the scenario reported in this paper, the screens used to create the particle showers were inserted at the same angle. Hence, assuming the same angle of incidence for the particles would be a reasonable approximation. The calibration factor, denoted as b related

to the attenuation by loss location, has been taken into account in both the data and simulation. For the calibration factor denoted as c, we assume it to be negligible as the tests are consecutive and involve low losses.

III. CHERENKOV OBLM IN CLEAR

A. CLEAR beam test facility

The CLEAR test facility provides a train of 220 MeV electron bunches with a maximum charge of 30 nC and bunch spacing of 666 ps [17] along 40 m of beam line. The line is equipped with several Beam TeleVision (BTV) screens that were used to generate controlled and intentional showers of losses. The BTVs at CLEAR are based on screens producing either optical transition radiation (OTR) from Silicon wafer or scintillation light from YAG. They are typically used for beam size and emittance measurements [18]. The dimensions of the BTVs used in the simulations and experiments of this study are (width × height × thickness) $20 \times 20 \times 0.5$ mm. Following the CLEAR beam line distribution, BTV390, BTV620, BTV730, and BTV810 were located at 20.55, 25.85, 29.75, and 32.60 m, respectively, considering the 0 m at the beam gun. In addition, a 1 m long In-Air stand is located before the dump at the end of the line. In this vacuum-free area, the beam path can be accessed directly during the experiments.

B. Capture angle setup

The photon capture factor was evaluated [19]. A 105 μm core diameter fiber of 2 m was installed on a rotating table placed directly in front of the beam path in the In-Air area. This configuration allowed the beam impact angle to be adjusted within the range between $(-80°, 80°)$, where 0° represents the position where the fiber is perpendicular to the beam. Both ends of the fiber were coupled to a module with different Silicon PhotoMultiplier (SiPM) photosensors (S14160-3010PS and S14160-3015PS) from Hamamatsu, through a FC-PC type connector. The boards were equipped with a LEMO connector for the SiPM bias voltage (42 V), GND and SMA connector for signal transmission to the oscilloscope.

Several photosensors could be utilized in this study, such as SiPMs or photomultiplier tubes (PMTs). Both devices have significant advantages and disadvantages that are worth considering. Among the limitations, SiPMs may exhibit cross-talk effect and saturation, while PMTs require high-voltage power and have substantially higher costs. The system reported in this paper is a prototype, tested at CLEAR facility, which is intended for use in other environments where we expect no saturation [8]. Then the SiPM was selected due to its ease of handling (requires no high voltage), cost-effectiveness and high sensitivity.

C. Longitudinal oBLM setup

In the Cherenkov oBLM setup implemented in CLEAR, two 200 μm core diameter fibers, of 63 and 37 m, made of silica material were installed parallel to the beam pipe at 10 cm far from the center of the beam line. Each fiber had one free end and one end coupled to the same module used in Section (III B), but using only the SiPM of S14160-3015PS series from Hamamatsu (with an operating voltage of 42 V). The 63 m length fiber measured the downstream signal, while the 37 m length fiber measured the upstream signal. The choice of the 3015PS series over the 3010PS was based on the number of pixels. The 3015PS had fewer pixels than the other, resulting in higher sensitivity in light collection. As the first BTV (BTV390) is located at the position 20.55 m in the line, only the second half of the accelerator needed to be covered by the fiber, therefore 21.75 m of the system was used as beam loss detector. The oscilloscope, power supplies, and photosensor modules were located in a technical gallery, above the accelerator hall, and the fibers were passed through separate holes in the ceiling.

IV. SIMULATIONS USING FLUKA

FLUKA comprises a wide range of routines written in FORTRAN 77, and they can be redesigned depending on simulation purposes. The simulations run a customized routine to provide an output file with valuable information about the charged secondary particles reaching the optical fiber. In this file, the user can find the particle type, the particle energy E, the velocity β, the position coordinates (X_i, Y_i, Z_i), the path traveled x_i inside of the fiber, and the impact angle ϕ_i with respect the z axis, i.e., the fiber axis. Additionally, the routine reduces the execution time of simulations by stopping the tracking of particles that do not reach predefined cuts. Only charged particles above the threshold velocity β_{th} will produce Cherenkov photons, neutral charge particles and slow particles will be discarded by default. Then our algorithm [10] collects all tracked particles reaching the fiber after cuts from the FLUKA output and solves Eq. (6), where the photon capture-transport probability and the photon attenuation are considered.

A. Expected signal as function of impacting angle

In the FLUKA simulations, the beam was configured as a 220 MeV electron beam with a rectangular momentum distribution and a Gaussian shape in its transverse coordinates ($\sigma_x = \sigma_y = 0.2$ cm). It impinged on the middle point of a 2 m long fiber with a core diameter of 105 μm. Charge was normalized to 25 pC per bunch. The angles of impact were set to the range $[10° - 80°]$ respect to the fiber axis. Considering the length of the fiber, the attenuation effect on the signal was discarded. Figure 4 compares the theoretical and simulated results of the expected signal

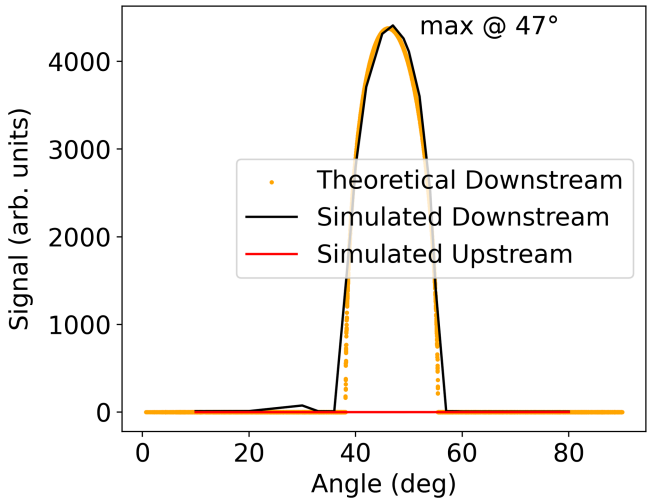

FIG. 4. Comparison between theoretical and simulated results of the expected photons with respect to the impact angles [8].

based on particle impact angles. Angle selection corresponds to the downstream fiber direction, and as expected, simulations indicate that there is no Cherenkov signal in the upstream direction. Simulated Cherenkov light emits with the same probability at the same range of angles as determined by the Cherenkov capture probability [Eq. (2)]. The maximum Cherenkov angle ($\theta \approx 47°$) matches with the angle of maximum capture probability.

B. Longitudinal oBLM System

As part of this section, we present a quantitative analysis of our proposed algorithm using FLUKA simulation results for Cherenkov photon generation. The FLUKA outcome is based on the beam losses caused by the insertion of BTV390, BTV620, BTV730, and BTV810 screens. The CLEAR geometry input included a 200 μm core diameter silica fiber implemented parallel to the beam pipe at a

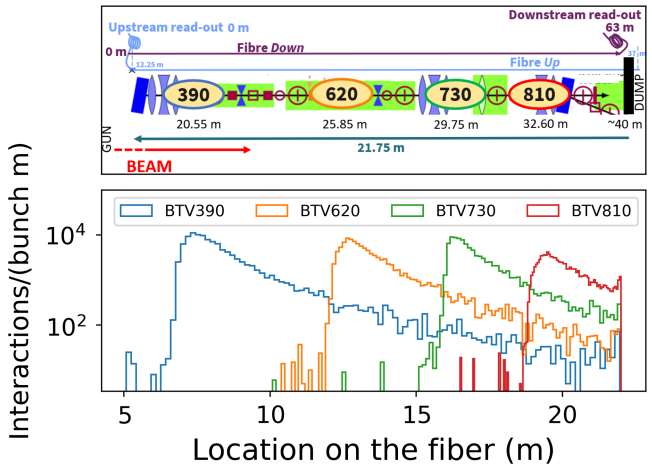

FIG. 5. Locations of the beam losses in the optical fiber caused by the different BTVs in CLEAR accelerator.

TABLE I. Approximated values of simulated Cherenkov photons expected at the oBLM from the beam losses from a CLEAR bunch (25 pC).

BTV	Photons/Bunch down[a]	Photons/Bunch up[b]
390	479 ± 30	13 ± 5
620	474 ± 30	10 ± 5
730	437 ± 40	9 ± 5
810	445 ± 20	9 ± 5

[a]The downstream direction follows the beam trajectory.
[b]The upstream direction is contrary to the beam trajectory.

distance of 10 cm, over the second half of the line (22 m approximately). The Gaussian electron beam used was set at 220 MeV. We adapted the material, dimensions, and locations of the screens used in the simulations to match those of the actual ones at the experimental site. Charge was normalized to 25 pC per bunch. Figure 5 presents the locations of the different showers of particles arriving at the optical fiber. The longitudinal distribution of the interactions is reported along the 22 m of fiber, approximately, along the second half of the beam line. The upper diagram shows the fiber setup. This distribution was selected considering the ceiling hole locations (where the fibers passed through to be connected to the readout), after verifying that area of interest of the line was sufficiently covered. The bottom plot shows the different signals for each screen.

Signals are produced within the wavelength range of [290, 900] nm, as established by the SiPM. In addition, the model is suitable for a quantitative calculation of the Cherenkov photons emitted in optical fibers due to loss detection. Table I collects the Cherenkov photons created per CLEAR bunch by the insertion of the BTVs. Based on their capture angle, photons are split into downstream and

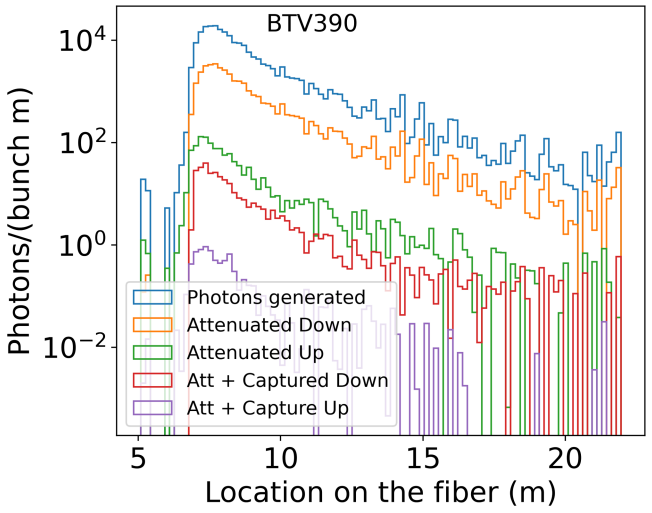

FIG. 6. Photon distribution of the losses caused by the BTV390 in CLEAR accelerator.

upstream quantities. Light attenuation is calculated by adding the lengths of the fibers (63 m for downstream and 37 m for upstream) and the location of the BTVs as inputs.

For completeness, the analysis includes the comparison between the total photons generated with the quantities of photons after the effects of attenuation and attenuation capture. Figure 6 shows the expected photon production comparing the three cases for the BTV390. As expected, the number of photons decreases with the factors.

V. EXPERIMENTAL VALIDATION

A. Results of angular scan

The fibers were mounted on a rotating table and remotely moved in steps of 3°–5° for both clockwise and anticlockwise movements (negative and positive angles, respectively). In Fig. 7, the results of an angular scan of a fiber with a core diameter of 105 micrometers are shown. Results are expressed over an average bunch charge of 25 pC. For silica fibers, the maximum values can be observed within the range $\theta = \pm[39°, 52°]$, despite the saturation.

B. Results of longitudinal loss location

The study also included estimations of loss locations along the CLEAR line. An illustration of the simulated and experimental upstream signals obtained in the photosensors as a result of the beam losses interacting with the optical fiber is shown in Fig. 8. Rising edges, or signal "knees" [20], were considered as photon arrival times at the SiPM. To achieve better signal amplitude, measurements with a five-bunched beam, 0.666 ns separated, are presented. The usage of trains of five consecutive bunches does not impact the curve "knee" time of the curves, which remains the same regardless of the number of bunches [8]. A threshold voltage value of −0.015 V was set in order to avoid background noise. Signals manifest in the expected sequence as they are generated along the fiber and there were no background

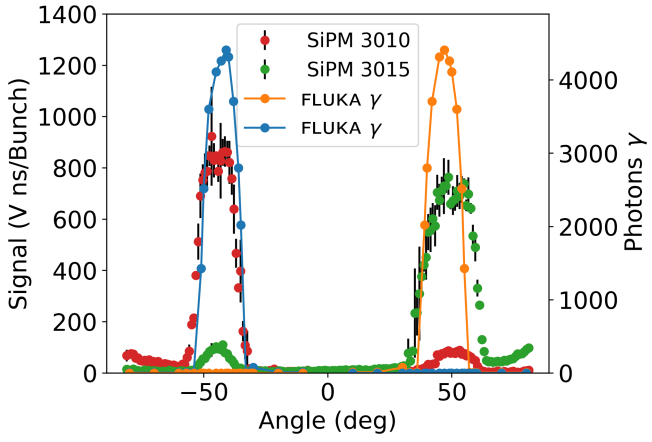

FIG. 7. Comparison between the light capture probabilities in CLEAR experiments and simulations [8].

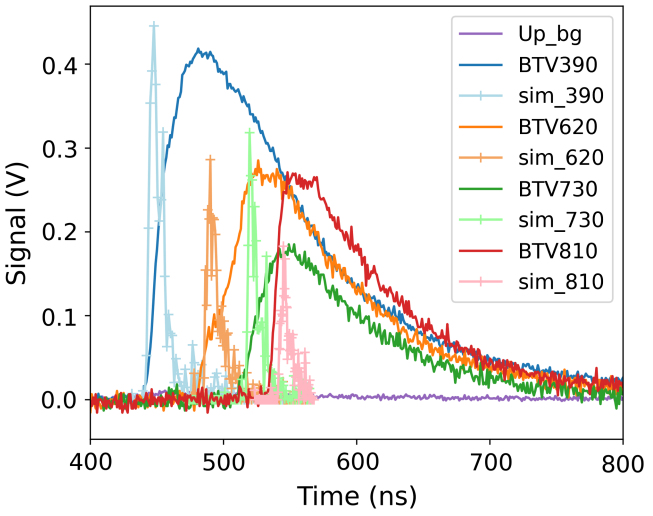

FIG. 8. Comparison between the simulated and experimental upstream signals measured from the collected photons during the generation of beam losses by inserting different BTVs in the CLEAR line.

peaks detected (indicated by a purple line labeled as Up_bg). Among the eight peaks, BTV390, BTV620, BTV730, and BTV810 represent the results derived from experimentation, while the remaining four peaks, sim_390, sim_620, sim_730, and sim_810, are the outputs yielded by simulation after attenuation and capture reductions. Due to the challenge of aligning both scenarios with a common reference point, a single adjustment factor has been applied to all the simulated peaks. This factor was calculated by comparing the signal and simulation peaks for the BTV390 screen and then applied to the rest of the simulated cases. The arrival times of the losses from each screen are identified as follows: $t_{390} = 440 \pm 2$ ns, $t_{620} = 481 \pm 1$ ns, $t_{730} = 512 \pm 2$ ns, and $t_{810} = 539 \pm 2$ ns. In order to normalize the amplitude of the peaks, a calibration value f_{cal} was computed based on the average of the maximum voltage-to-photon ratios. The value of this factor is $f_{\text{cal}} = 0.96$ V/photon.

Note that the experimental signals show peak broadening caused by rise and fall times introduced by the photosensors. Also, extra width might be produced by differences in the shower distribution due to the multibunch structure. These effects are not taken into account in the simulations.

In Table II, we summarize the results obtained by applying Eq. (7b), using real values such as distances d_{R} and expected photon traveling times t_{R} between screens. These values are compared with the time intervals Δt_{Up} obtained from the differences in arrival times between upstream signals and the estimated distances between the various screens.

Several complexities were identified during the analysis of downstream signals. From Eq. (7), we derive the factor $(1+n)/(1-n) = -5.35$ (for $n = 1.46$), which gives the difference in the temporal separation of the signals at the

TABLE II. Beam loss location results from the upstream arrival time difference in the BTVs scans.

Screens	Real distance d_R (m)	Expected[a] time t_R (ns)	Signal time interval Δt_{Up} (ns)	Estimated distance d (m)
390–620	5.3	43.5	41 ± 3	5.0 ± 0.4
620–730	3.9	32.0	31 ± 3	3.9 ± 0.4
730–810	2.85	23.4	27 ± 4	2.9 ± 0.5

[a]Arrival time of a photon from one screen to another, travelling a distance d_R.

upstream and downstream ends. The negative sign implies a reversal in the arrival times of the loss signals. For instance, for a loss location $\Delta x = 1$ m, the arrival time at the upstream end would be $\Delta t_{Up} = 8.2$ ns and the arrival time at the downstream end $\Delta t_{Down} = -1.53$ ns. Consequently, downstream signals exhibit not only a worse resolution than the upstream signal but also a less well-defined timing reference. For the upstream signal, the timing reference point is clearly indicated by the time of the curve knee of the arriving signals, and it is also possible to follow the chronological order of each shower of particles. In contrast, for the downstream signal, the timing reference point could be smeared due to the difference in the speed between the beam particles in a vacuum and the photons in the fibre. For instance, in a hypothetical situation where a particle shower A is produced followed by a particle shower B, photons created inside the fiber by shower A would be created first but they would arrive at the photosensor after the "knee" time of the signal of the photons from B. This is due to the fact that particles in B travel at a velocity $\approx c$ while photons propagate at a velocity $\approx c/n$ [21]. Therefore, the signal arrival times might not correspond to the expected particle shower but to a particle shower produced further downstream. Hence, comparing upstream and downstream signals and determining loss locations through downstream signals become more complex and require further investigation. However, the use of the upstream sensor has been proven to provide beam loss location with less than a meter of uncertainty.

VI. CONCLUSION

The paper presents an in-depth examination of Cherenkov Optical Beam Loss Monitors (oBLMs) and their potential application in particle accelerators. Utilizing FLUKA software, simulations were conducted to analyze the generation and propagation of Cherenkov photons within optical fibers. A model for Cherenkov photon generation inside these fibers was developed to incorporate factors related to photon capture and attenuation. Experimental measurements conducted at CLEAR confirmed the simulations, particularly concerning anticipated photon behaviors in relation to impact angles and longitudinal loss location. Notably, the highest generation angle, $\theta_{c,max} \approx 47°$, was observed for silica fibers. These experiments also underscored the oBLM system's capacity to accurately pinpoint beam losses along the accelerator beam line, achieving a resolution of under half a meter. The integration of these technologies holds significant promise in bolstering accelerator safety and performance.

ACKNOWLEDGMENTS

We acknowledge the support and collaboration of the SY-BI-BL and SY-BI-PM CERN sections during the development of the electronic modules and the setup of the experiments and also the CLEAR team for its invaluable assistance during the installation and execution of the tests.

[1] A. S. Fisher, C. I. Clarke, B. T. Jacobson, R. Kadyrov, E. Rodriguez, M. Santana Leitner, L. Sapozhnikov, and J. J. Welch, Beam-loss detection for the high-rate superconducting upgrade to the SLAC linac coherent light source, Phys. Rev. Accel. Beams **23**, 082802 (2020).

[2] K. Wittenburg, *Beam Loss Monitors* (2020), https://api.semanticscholar.org/CorpusID:170077093.

[3] M. Kastriotou, Optimisation of storage rings and RF accelerators via advanced optical-fibre based detectors, Ph.D. thesis, University of Liverpool, 2018.

[4] C. Ahdida *et al.*, New capabilities of the FLUKA multipurpose code, Front. Phys. **9**, 788253 (2022).

[5] V. Vlachoudis, FLAIR: A powerful but user friendly graphical interface for FLUKA, in *Proceedings of the International Conference on Mathematics, Computational Methods and Reactor Physics* (Saratoga Springs, New York, 2009).

[6] I. Tamm, Radiation emitted by uniformly moving electrons, in *Selected Papers* (Springer Berlin Heidelberg, Berlin, Heidelberg, 1991), pp. 37–53.

[7] K. Nakamura, Review of particle physics, J. Phys. G **37**, 075021 (2010).

[8] S. Benitez, Design and development of an optical beam loss monitor based on Cherenkov light detection for the CERN Super Proton Synchrotron Accelerator, Ph.D. thesis, School of Computing and Engineering, 2022.

[9] D. Gamba *et al.*, The CLEAR user facility at CERN, Nucl. Instrum. Methods Phys. Res., Sect. A **909**, 480 (2018).

[10] S. Benitez, Cherenkov Light Generation Tool, https://gitlab.cern.ch/sbenitez/cherenkov_light_generation_model (2022).

[11] G. Agrawal, *Fiber-Optic Communication Systems*, Wiley Series in Microwave and Optical Engineering (Wiley, New York, 2012).

[12] S. H. Law, S. C. Fleming, N. Suchowerska, and D. R. McKenzie, Optical fiber design and the trapping of Čerenkov radiation, Appl. Opt. **45**, 9151 (2006).
[13] It could be simplified by noticing that $\sqrt{n_{co}^2 - NA^2} = n_{cl}$, however, both NA and n_{co} values are more commonly facilitated by manufacturers.
[14] Equation (2) considers skew and meridional rays crossing the fiber. Skew rays are transmitted through the fiber following a helical path while the meridional ones cross the fiber axis [11].
[15] M. E. Wandel, Attenuation in silica-based optical fibers, Ph.D. thesis, Technical University of Denmark, Copenhagen, Denmark, 2005.
[16] K. Tsujikawa, K. Tajima, and M. Ohashi, Rayleigh scattering reduction method for silica-based optical fiber, J. Lightwave Technol. **18**, 1528 (2000).
[17] R. Corsini, L. Dyks, W. Farabolini, A. Gilardi, P. Korysko, and K. Sjobak, Status of VHEE radiotherapy related studies at the CLEAR User Facility at CERN, in *Proceedings of the 12th International Particle Accelerator Conference, Campinas, SP, Brazil* (JACoW, Geneva, Switzerland, 2021), WEPAB044.
[18] E. Bravin, S. Burger, G. Ferioli, G. J. Focker, A. Guerrero, and R. MacCaferri, A new TV beam observation system for CERN, in *Proceedings of the 7th European Workshop on Beam Diagnostics and Instrumentation for Particle Accelerators, DIPAC 2005, Lyon, France* (JACoW, Geneva, Switzerland, 2005).
[19] S. Benitez, E. Effinger, W. Farabolini, A. Gilardi, P. Korysko, P. Lane, E. Lima, B. Salvachúa, and W. Viganò, Development and testing of a Cherenkov beam loss monitor in CLEAR Facility, in *Proceedings of the 12th International Particle Accelerator Conference, Campinas, SP, Brazil* (JACoW, Geneva, Switzerland, 2021).
[20] In the signal, the time at which the peak begins to rise from the baseline.
[21] It corresponds to the silica refractive index of $n = 1.46$.